NASA/CR-2013-217911

Range-specific High-resolution Mesoscale Model Setup

Leela R. Watson
ENSCO, Inc., Cocoa Beach, Florida
NASA Applied Meteorology Unit, Kennedy Space Center, Florida

January 2013

NASA STI Program ... in Profile

Since its founding, NASA has been dedicated to the advancement of aeronautics and space science. The NASA scientific and technical information (STI) program plays a key part in helping NASA maintain this important role.

The NASA STI program operates under the auspices of the Agency Chief Information Officer. It collects, organizes, provides for archiving, and disseminates NASA's STI. The NASA STI program provides access to the NASA Aeronautics and Space Database and its public interface, the NASA Technical Reports Server, thus providing one of the largest collections of aeronautical and space science STI in the world. Results are published in both non-NASA channels and by NASA in the NASA STI Report Series, which includes the following report types:

- TECHNICAL PUBLICATION. Reports of completed research or a major significant phase of research that present the results of NASA Programs and include extensive data or theoretical analysis. Includes compilations of significant scientific and technical data and information deemed to be of continuing reference value. NASA counterpart of peer-reviewed formal professional papers but has less stringent limitations on manuscript length and extent of graphic presentations.

- TECHNICAL MEMORANDUM. Scientific and technical findings that are preliminary or of specialized interest, e.g., quick release reports, working papers, and bibliographies that contain minimal annotation. Does not contain extensive analysis.

- CONTRACTOR REPORT. Scientific and technical findings by NASA-sponsored contractors and grantees.

- CONFERENCE PUBLICATION. Collected papers from scientific and technical conferences, symposia, seminars, or other meetings sponsored or co-sponsored by NASA.

- SPECIAL PUBLICATION. Scientific, technical, or historical information from NASA programs, projects, and missions, often concerned with subjects having substantial public interest.

- TECHNICAL TRANSLATION. English-language translations of foreign scientific and technical material pertinent to NASA's mission.

Specialized services also include organizing and publishing research results, distributing specialized research announcements and feeds, providing information desk and personal search support, and enabling data exchange services.

For more information about the NASA STI program, see the following:

- Access the NASA STI program home page at http://www.sti.nasa.gov

- E-mail your question to help@sti.nasa.gov

- Fax your question to the NASA STI Information Desk at 443-757-5803

- Phone the NASA STI Information Desk at 443-757-5802

- Write to:
  STI Information Desk
  NASA Center for AeroSpace Information
  7115 Standard Drive
  Hanover, MD 21076-1320

NASA/CR-2013-217911

Range-specific High-resolution Mesoscale Model Setup

Leela R. Watson
ENSCO, Inc., Cocoa Beach, Florida
NASA Applied Meteorology Unit, Kennedy Space Center, Florida

National Aeronautics and
Space Administration

Kennedy Space Center
Kennedy Space Center, FL 32899-0001

January 2013

Acknowledgements

The author thanks Mr. William Roeder of the 45th Weather Squadron and Mr. Theodore Wilz of the Wallops Flight Facility for providing input and valuable feedback on the overall direction of this task, and Dr. William Bauman, Ms. Winifred Crawford and Ms. Jaclyn Shafer of the Applied Meteorology Unit for their assistance in the completion of this task.

Available from:

NASA Center for AeroSpace Information
7115 Standard Drive
Hanover, MD 21076-1320
443-757-5802

This report is also available in electronic form at

http://science.ksc.nasa.gov/amu/

Executive Summary

Mesoscale weather conditions can have an adverse effect on space launch, landing, ground processing, and weather advisories, watches, and warnings at the Eastern Range (ER) in Florida and Wallops Flight Facility (WFF) in Virginia. During summer, land-sea interactions across Kennedy Space Center (KSC) and Cape Canaveral Air Force Station (CCAFS) lead to sea breeze front formation, which can spawn deep convection that can hinder operations and endanger personnel and resources. Many other weak locally-driven low-level boundaries and their interactions with the sea breeze front and each other can also initiate deep convection in the CCAFS/KSC area. These convective processes often last 60 minutes or less and pose a significant challenge to the local forecasters. Surface winds during the transition seasons (spring and fall) pose the most difficulties for the forecasters at WFF. They also encounter problems forecasting convective activity and temperature during those seasons. Therefore, accurate mesoscale model forecasts are needed to better forecast a variety of unique weather phenomena. Global and national scale models cannot properly resolve important local-scale weather features at each location due to their horizontal resolutions being much too coarse. Therefore, a properly tuned model at a high resolution is needed to provide improved capability. To accomplish this, the ER and WFF supported the tasking of the Applied Meteorology Unit (AMU) to perform a number of sensitivity tests in order to determine the best model configuration for operational use at each of the ranges to best predict winds, precipitation, and temperature.

The AMU compared model forecasts for both the ER and WFF using different Weather Research and Forecasting (WRF) model dynamical cores, grid configurations, and physical schemes to determine the impact on model skill. Different model configurations were tested by varying the dynamical core, grid spacing, domain size, and forecast length. This enabled the AMU to determine the optimal configuration that allowed for the largest domain size and highest resolution to capture unique weather phenomena with the shortest wall-clock run time. Once the configurations were chosen, the AMU varied the model physics to determine which produced the best forecasts. The WRF model forecasts were validated using simple statistics that compared locally available observational surface and upper air data to the forecast data. The objective statistical analysis included the model bias, mean error, and the root mean square error. Precipitation forecasts were compared to nationally available rainfall data using the Method for Object-Based Diagnostic Evaluation (MODE), a technique developed at the National Center for Atmospheric Research.

The AMU ran test cases in the warm and cool seasons at the ER and for the spring and fall seasons at WFF. For both the ER and WFF, the Advanced Research WRF core outperformed the Non-hydrostatic Mesoscale Model core. Results for the ER indicate that the Lin microphysical scheme and the Yonsei University (YSU) planetary boundary layer (PBL) scheme is the optimal model configuration for the ER. It consistently produced the best surface and upper air forecasts, while performing fairly well for the precipitation forecasts. Both the Ferrier and Lin microphysical schemes in combination with the YSU PBL scheme performed well for WFF in the spring and fall seasons.

Future work under the multi-year AMU modeling tasks will provide a recommended local data assimilation and numerical forecast model design optimized for both the ER and WFF to support space launch activities. The AMU will determine the best software and type of assimilation to use, as well as determine the best grid resolution for the initialization based on spatial and temporal availability of data and the wall clock run-time of the initialization. The AMU will transition from the WRF EMS to NU-WRF, a NASA-specific version of the WRF that takes advantage of unique NASA software and datasets.

Table of Contents

Executive Summary 2

List of Figures 4

List of Tables 5

1. Introduction 7
   - 1.1 Background Information 7
   - 1.2 Mesoscale Model Core Options 8
   - 1.3 Model Physics Options 8
   - 1.4 Report Format and Outline 10

2. Eastern Range 10
   - 2.1 Model Configuration and Test Cases 10
   - 2.2 Forecast Validation 13
   - 2.3 Warm Season Results 16
   - 2.4 Cool Season Results 20
   - 2.5 Additional Comparisons 23
   - 2.6 Recommendations 23

3. Wallops Flight Facility 24
   - 3.1 Model Configuration and Test Cases 24
   - 3.2 Forecast Validation 27
   - 3.3 Fall Season Results 30
   - 3.4 Spring Season Results 33
   - 3.5 Recommendations 35

References 38

List of Figures

Figure 1. Map of east-central Florida showing the model domain boundaries. The red square shows the outer domain and the yellow square the inner domain for all configurations regardless of horizontal resolution or domain core. 13

Figure 2. Seven KSC/CCAFS wind towers that were used to validate the WRF forecasts on the ER (shown in red). The XMR RAOB site used to validate the upper air forecasts is shown in yellow. 14

Figure 3. Map of the Delmarva Peninsula showing the WRF ARW model domain boundaries. The red square shows the outer 4 km domain and the yellow square the inner 1.33 km domain. 25

Figure 4. Map of the Delmarva Peninsula showing the WRF NMM model domain boundaries. The red square shows the outer 3 km domain and the yellow square the inner 1 km domain. 26

Figure 5. Seven METAR (shown in red) and four buoy (shown in green) weather reporting stations that were used to validate the WRF forecasts for WFF..... 28

List of Tables

Table 1. List of additional physics options used for each model run for both the ARW and NMM cores. 12

Table 2. GBN chart of the average 30-day ME for August 2011 for all seven KSC/CCAFS wind towers for the three initial WRF configurations and two national models. 17

Table 3. GBN chart of the average 30-day ME and RMSE for 1-30 August 2011 for all seven KSC/CCAFS wind towers for the three initial WRF configurations. 17

Table 4. GBN totals from the ME and RMSE values for the three initial WRF configuration forecasts at the seven wind towers during 1-30 August 2011. 18

Table 5. GBN chart of the average ME and RMSE for 1-7 August 2011 for all seven KSC/CCAFS wind towers for the six ARW configurations. 18

Table 6. GBN totals from the ME and RMSE values for the six ARW configuration forecasts at the seven wind towers during 1-7 August 2011. 19

Table 7. GBN chart of the average ME and RMSE for 1-7 August 2011 for the 2200 UTC XMR RAOB for the six ARW configurations. 19

Table 8. GBN chart for the average 30-day MODE statistics for 1-30 August 2011 over the ER WRF domain for the initial three WRF configurations. 20

Table 9. GBN chart for the average MODE statistics for 1-7 August 2011 over the ER WRF domain for the six ARW configurations. 20

Table 10. GBN chart of the average ME and RMSE for 18-25 February 2012 for four KSC/CCAFS wind towers for the three initial WRF configurations and two national models. 21

Table 11. GBN totals from the ME and RMSE values for the three initial WRF configurations and two national models at the four wind towers during 18-25 February 2012. 22

Table 12. GBN chart for the average MODE statistics for 18-25 February 2012 over the ER WRF domain. 22

Table 13. GBN chart of the average ME and RMSE for 18-25 February 2012 for four KSC/CCAFS wind towers for three ARW configurations with varying horizontal resolutions. 23

Table 14. List of additional physics options used for each model run for both the ARW and NMM cores. 27

Table 15. GBN chart of the average 7-day ME and RMSE for 1-7 November 2011 for three METAR sites for four WRF configurations and one national model. 31

Table 16. GBN totals from the ME and RMSE values for the four WRF and one national model forecasts at the three METAR sites during 1-7 November 2011. 31

Table 17. GBN chart of the average ME and RMSE for 1-14 November 2011 for all seven METAR and four buoy sites for three ARW configurations. 32

Table 18. GBN totals from the ME and RMSE values for the three ARW forecasts at all seven METAR and four buoy sites during 1-14 November 2011. 32

Table 19. GBN chart of the average ME and RMSE for 1-14 November 2011 for the 0000 and 1200 UTC KWAL RAOB for the three ARW configurations. 33

Table 20. GBN chart for the average 14-day MODE statistics for 1-14 November 2011 over the WFF WRF domain for the three ARW configurations. 33

Table 21. GBN chart of the average 30-day ME for 1-30 April 2012 for all seven METAR and four buoy sites for three ARW configurations. 34

Table 22. GBN totals from the ME and RMSE values for the three ARW forecasts at the seven METAR and four buoy sites during 1-30 April 2012. 34

Table 23. GBN chart of the average ME and RMSE for 1-30 April 2012 for the 0000 and 1200 UTC KWAL RAOB for the three ARW configurations. 35

Table 24. GBN chart for the average 30-day MODE statistics for 1-30 April 2012 over the WFF WRF domain. 35

1. Introduction

Mesoscale weather conditions can have an adverse effect on space launch, landing, ground processing, and weather advisories, watches, and warnings at the Eastern Range (ER) in Florida and Wallops Flight Facility (WFF) in Virginia. During summer, land-sea interactions across Kennedy Space Center (KSC) and Cape Canaveral Air Force Station (CCAFS) lead to sea breeze front formation, which can spawn deep convection that can hinder operations and endanger personnel and resources. Many other weak locally-driven low-level boundaries and their interactions with the sea breeze front and each other can also initiate deep convection in the CCAFS/KSC area. Some of these other boundaries include the Indian River Breeze front, Banana River Breeze front, outflows from previous convection, horizontal convective rolls, convergence lines from other inland bodies of water such as Lake Okeechobee, the Trailing Convergence Line from convergence of sea breeze fronts due to the shape of Cape Canaveral, frictional convergence lines from the Bahamas Islands, convergence lines from soil moisture differences, convergence lines from cloud shading, and others. All these subtle weak boundary interactions often make forecasting of operationally important weather very difficult at CCAFS/KSC during the summer. These convective processes often build quickly, last a short time (60 minutes or less), and occur over small distances, all of which also poses a significant challenge to the local forecasters. Surface winds during the transition seasons (spring and fall) pose the most difficulties for the forecasters at WFF. They also encounter problems forecasting convective activity and temperature during those seasons. Therefore, accurate mesoscale model forecasts are needed to aid in their decision making.

Both the ER and WFF would benefit greatly from high-resolution mesoscale model output to better forecast a variety of unique weather phenomena. Global and national scale models cannot properly resolve important local-scale weather features at each location due to their horizontal resolutions being much too coarse. Therefore, a properly tuned model at a high resolution is needed to provide improved capability. This task is a multi-year study in which the Weather Research and Forecasting (WRF) model will be tuned individually for each range. The goal of the first year, the results of which are in this report, was to tune the WRF model based on the best model resolution and run time while using reasonable computing capabilities. To accomplish this, the ER and WFF supported the tasking of the Applied Meteorology Unit (AMU) to perform a number of sensitivity tests in order to determine the best model configuration for operational use at each of the ranges to best predict winds, precipitation, and temperature.

1.1 Background Information

A number of studies have been conducted on model forecast sensitivities to different parameters. Most studies were conducted for a specific area or particular meteorological phenomena. The importance of a comprehensive and accurate analysis of the state of the atmosphere for the forecast initial conditions is vital to improving model skill. Cheng et al. (2010) notes that mesoscale weather phenomena are very sensitive to the atmospheric physical processes and that model physics schemes should be carefully evaluated when setting up a forecasting system. Their study found that, although the model physics is important, it played a secondary role to the synoptic environment, which must be well simulated in order to produce a good mesoscale forecast.

It is well known that warm season rainfall is very challenging to predict (Olson et al. 1995). A study conducted by Jankov et al. (2005) found that the choice of a microphysical scheme impacted the total rain volume of warm season convection. Gallus and Bresch (2006) extended these results and found that:

- forecasted peak summer rain rates over the United States were more sensitive to the physics package than to the dynamical core,
- total rain volume was more sensitive to the dynamical core than the physics, and
- both the physics and dynamical core had a greater impact on the forecasts than the initial conditions that were chosen.

1.2 Mesoscale Model Core Options

The WRF numerical weather modeling system is a next-generation mesoscale forecast model that can be used for a wide range of applications with an emphasis on horizontal grid sizes in the range of 1-10 km (Tao et al. 2011). It consists of two dynamical cores, Advanced Research WRF (ARW) and Non-hydrostatic Mesoscale Model (NMM). The ARW core was developed primarily at the National Center for Atmospheric Research (NCAR) while the NMM was developed at the National Centers for Environmental Prediction (NCEP). The work described in this report employed the WRF Environmental Modeling System (EMS) software, which was developed by the National Weather Service (NWS) Science and Operations Officer (SOO) Science and Training Resource Center (STRC; http://strc.comet.ucar.edu/software/newrems). A benefit of using the WRF EMS is that it incorporates both dynamical cores into a single end-to-end forecasting model (Rozumalski 2006). The software consists of pre-compiled programs that are easy to install and run.

For this study, the AMU compared forecasts from both the ARW and NMM cores of the WRF model. The ARW core is a fully compressible, non-hydrostatic mesoscale model with a hydrostatic option. It consists of a mass-based hydrostatic pressure terrain following coordinate, Arakawa C-grid staggering for the horizontal grid, time-split integration using a third order Runge-Kutta scheme with a small step for acoustic and gravity wave modes, and up to sixth order advection options in the horizontal and vertical (Skamarock et al. 2005). There are also full physics options for microphysics, planetary boundary layer, cumulus parameterization, radiation, and land surface schemes (Skamarock et al. 2005). The NMM core is also a fully compressible, non-hydrostatic mesoscale model with a hydrostatic option (Janjic et al. 2001, Janjic 2003a, b). It consists of a hybrid sigma-pressure, terrain following vertical coordinate, Arakawa E-grid, a forward-backward time integration scheme, a second order advection option in the horizontal and vertical, and conservation of energy and enstrophy (Janjic 1984). Most physics packages available to the ARW are also available to the NMM, but a majority of them have not been tested or have undergone preliminary testing only with the NMM. Therefore, the physics options for the NMM are more limited than for the ARW.

1.3 Model Physics Options

The WRF model offers a choice of many different physics options including schemes for boundary layer, surface layer, radiation, microphysics, turbulence, and cumulus parameterization. For this task, different microphysical and planetary boundary layer schemes were compared since they offered the most varied options. While a full comparison of all the physics would have been ideal, time constraints limit the comparison to a select group that, based on a literature review, are the most widely used within the modeling community and/or have been shown to produce the best results. The following provides a brief description of each of the model physics options that were tested in this task.

1.3.1 Microphysical Schemes

Microphysics schemes are important for accurately modeling cloud process to correctly simulate the state of the atmosphere. Microphysics schemes in the WRF model explicitly

resolve various forms of water at a grid point including vapor, cloud water, cloud ice, rain, snow, and hail. Some of the microphysics schemes available in WRF include all of these forms, while others exclude some of them. Three microphysical algorithms that include all forms of water were tested in this task and are described below: Lin, Ferrier, and WDM6.

The Lin scheme is based on Lin et al. (1983), Rutledge and Hobbs (1984), and Chen and Sun (2002) and is a two-dimensional scheme. It predicts cloud water, cloud ice, water vapor, rain, snow, and graupel at each grid point based on advection, production, and fallout. It uses the “bulk water” parameterization technique to represent precipitation fields that are all assumed to follow exponential size distribution functions (Lin et al. 1983). It is considered a sophisticated microphysics scheme in WRF and is suitable for real-data high-resolution simulations. It was added to the WRF model in 2000.

The Ferrier scheme predicts changes in water vapor and total condensate in the forms of cloud water, cloud ice, rain, and precipitation ice (snow, graupel, and sleet). The model advects the water vapor and total condensate, which is made up of the individual hydrometeor fields, making it computationally efficient. The Ferrier scheme also uses the bulk water parameterization technique. It is used in the operational NCEP models and was added to the WRF model in 2000.

The WRF Double-Moment 6-Class (WDM6) scheme was developed by Lim and Hong (2010) and is based on the WRF Single-Moment 6-Class (WSM6) scheme. It predicts the mixing ratios of water vapor, cloud water, cloud ice, rain, snow and graupel as in the WSM6 scheme, as well as the prognostic variables of cloud, rain water, and cloud condensation nuclei number concentrations. This scheme was added to the WRF model in 2009.

1.3.2 Planetary Boundary Layer Schemes

Planetary boundary layer (PBL) schemes play a critical role in simulating the boundary layer by parameterizing the vertical turbulent sub-grid scale fluxes in the PBL and the atmospheric column as a whole. The schemes determine the flux profiles in the boundary layer and stable layer above and provide vertical atmospheric tendencies of temperature, moisture, and horizontal momentum (Hu et al. 2010). Therefore, these PBL schemes are important for forecasting the initiation of convection and wind. A closure scheme is needed to determine the turbulent fluxes from the mean variables (Holt and Raman 1988, Hu et al. 2010). PBL schemes are generally divided into first-order or 1.5 order, also known as turbulent kinetic energy (TKE), closure schemes. First order closure schemes do not require additional prognostic equations to determine the effects of turbulence on the mean variables while 1.5 order (TKE) scheme requires an additional prognostic equation of the TKE (Shin and Hong 2011). The AMU tested three PBL algorithms in this task and they are described below: Mellor-Yamada-Janjic (MYJ), Yonsei University (YSU) and NCEP Global Forecast System (GFS).

The MYJ PBL scheme is a TKE closure scheme that requires one additional prognostic equation of TKE and uses the Mellor-Yamada Level turbulence closure model to represent turbulence above the surface layer (Mellor and Yamada 1982 and Janjic 1990, 1996, 2002). It determines the eddy diffusion coefficients from prognostically calculated TKE.

The YSU PBL scheme is a first-order closure scheme that is an update of the Medium-Range Forecast (MRF) PBL scheme (Hong and Pan 1996). It relies heavily on the Richardson number (Ri) to compute the PBL height for stable, unstable and neutral PBLs. The PBL height under this scheme is the point at which an Ri of 0.0 is reached.

The NCEP GFS PBL scheme is also a first-order vertical diffusion scheme that is closely related to the MRF PBL scheme. This scheme is used operationally at NCEP. More details can be found in Troen and Mahrt (1986) and Hong and Pan (1996).

1.4 Report Format and Outline

This report presents the findings from a study of model sensitivities for predicting unique weather phenomena at the ER and WFF. This analysis examined different dynamical cores, grid configurations, and physical schemes to determine the impact on model skill. The AMU assessed model skill by using an objective statistical analysis that included the mean error (ME) and the root mean square error (RMSE). Precipitation forecasts were evaluated using the Method for Object-Based Diagnostic Evaluation (MODE). Section 2 describes the model configuration, forecast validation technique, warm season and cool season results, and recommendations for the ER. Section 3 describes the model configuration, forecast validation technique, fall and spring season results, and recommendations for WFF. Each section is written to be a stand-alone guide for each range.

2. Eastern Range

This section describes the model configuration and test cases, results, and recommendations for an operational model for the ER.

2.1 Model Configuration and Test Cases

The most important part of this task was the model configuration. The ER wanted an operational model that could offer them information that is not readily available from national models. This included

- a higher resolution model that could run at a more frequent interval than the national models,
- a model that could output forecast data at a more frequent interval,
- a model that could be configured for the unique weather patterns in east-central Florida, and
- all of the above being feasible in an operational time frame.

To meet these requirements, the AMU tested various WRF model configurations by varying the dynamical core, grid spacing, domain size, and forecast length. This enabled the AMU to determine the optimal configuration that allowed for the largest domain size and highest resolution necessary to capture unique weather phenomena on the ER with the shortest wall-clock run time.

The AMU conducted testing on a 6-year old local modeling cluster that consists of 24 nodes/48 processors. To estimate how the model would run on more modern equipment, the AMU scaled the model run-time information to that of a newer, faster cluster with similar specifications. The domain size or resolution may be further increased depending on the specifications of the cluster used to run the WRF model. In addition, the adaptive time-step option was turned on in the WRF model. The time-step length is a user-configurable parameter that normally remains constant throughout the model run. Choosing an appropriate time-step is important since one that is too long will cause instability and/or model failure and one that is too short is a waste of computing power. The adaptive time-step allows the time-step to be varied as necessary through the simulation to improve model performance and reduce the instability. Model run-time can be reduced using this option.

Choosing one model configuration that would best fit the requirements was not a linear process. The AMU first chose two preliminary domain configurations using the NMM core for testing. Initially, the NMM was chosen over the ARW due to the significantly faster run-time. After running these two configurations and validating the results, the AMU decided to compare an ARW configuration as well. Results from those tests indicated that the ARW configuration produced a better overall forecast than the two NMM configurations. Based on these findings, the AMU decided to run the ARW with different physics options and compare the results. At the end of the testing process, forecasts from the following 10 configurations[1], two NMM and eight ARW, were compared:

Configuration 1: NMM core, 3 km outer domain and 1 km inner domain, Ferrier microphysics scheme, MYJ PBL scheme (NMM 3/1),

Configuration 2: NMM core, 2 km outer domain and 0.67 km inner domain, Ferrier microphysics scheme, MYJ PBL scheme (NMM 2/0.6),

Configuration 3: ARW core, 2 km outer domain and 0.67 km inner domain, Lin microphysics scheme, YSU PBL scheme (Lin-YSU),

Configuration 4: ARW core, 2 km outer domain and 0.67 km inner domain, Ferrier microphysics scheme, YSU PBL scheme (Ferrier-YSU),

Configuration 5: ARW core, 2 km outer domain and 0.67 km inner domain, WDM6 microphysics scheme, YSU PBL scheme (WDM6-YSU),

Configuration 6: ARW core, 2 km outer domain and 0.67 km inner domain, Goddard microphysics scheme, YSU PBL scheme (Goddard-YSU),

Configuration 7: ARW core, 2 km outer domain and 0.67 km inner domain, Ferrier microphysics scheme, MYJ PBL scheme (Ferrier-MYJ),

Configuration 8: ARW core, 2 km outer domain and 0.67 km inner domain, WDM6 microphysics scheme, MYJ PBL scheme (WDM6-MYJ),

Configuration 9: ARW core, 2 km outer domain and 0.67 km inner domain, Ferrier microphysics scheme, NCEP GFS PBL scheme (Ferrier-GFS),

Configuration 10: ARW core, 2 km outer domain and 0.67 km inner domain, WDM6 microphysics scheme, NCEP GFS PBL scheme (WDM6-GFS).

All other physics parameters were the same for each ARW model run. The NMM runs did not use the same physics as the ARW runs since physics options are more limited for the NMM. Table 1 lists the physics options used in both the ARW and NMM runs that were held constant. Note that cumulus parameterization schemes are generally not used with grid spacing that is less than 3 km.

[1] Model configurations will be referenced by their name in parentheses in the results sections (2.3 and 2.4).

Table 1. List of additional physics options used for each model run for both the ARW and NMM cores.

Physics Option	ARW	NMM
Cumulus Parameterization	None	None
Land surface option	Noah Land Surface Model (Chen and Dudhia 2001)	Noah Land Surface Model (Chen and Dudhia 2001)
Shortwave radiation scheme	Dudhia (Dudhia 1989)	GFDL (Lacis and Hansen 1974)
Longwave radiation scheme	RRTM (Mlawer et al. 1997)	GFDL (Fels and Schwarzkopf 1975; Schwarzkopf and Fels 1985, 1991)

Figure 1 shows domain size of both the inner and outer grid for each of the WRF configurations. The outer grid had the larger spacing (3 or 2 km) and the inner grid had smaller spacing (1 or 0.67 km) between grid points. Although the grid resolutions and dynamical core varied among the different configurations, the domain sizes for each configuration were roughly the same.

The AMU ran each model simulation at the specified horizontal resolution with 45 irregularly spaced, vertical sigma levels up to 50 mb. For the warm season, each run was initiated at 1500 UTC and integrated 9 hours once per day using the 12 km North American Mesoscale (NAM) model for boundary and initial conditions. Test cases from August 2011 were run to see if the model was able to capture the warm season convective initiation, onset of the sea breeze, and other warm season phenomena. Configurations 1-3 were run for the entire month of August 2011. Configurations 4-10 were run from 1-7 August 2011 instead of the whole month due to time constraints.

Configurations 1, 3, and 4 were chosen to compare results in the cool season based on the results from the warm season model runs. Configurations 3 and 4 performed consistently well (see Section 2.3), while Configuration 1 was included to determine if the NMM performed better in the cool season. The AMU ran test cases for the three configurations for 18-25 February 2012. Two 9-hour forecasts were initialized each day at 0000 and 1200 UTC using the 12 km NAM model for boundary and initial conditions, Short-term Prediction Research and Transition Center (SPoRT) Land Information System (LIS) land surface data, and SPoRT sea surface temperature (SST) data. The LIS and SST data were not used in the warm season comparison as the AMU did not have the archive data available. Two 9-hour forecasts were run in the cool season in order to capture a variety of phenomena including synoptic systems, frontal passages, and cool winter nights.

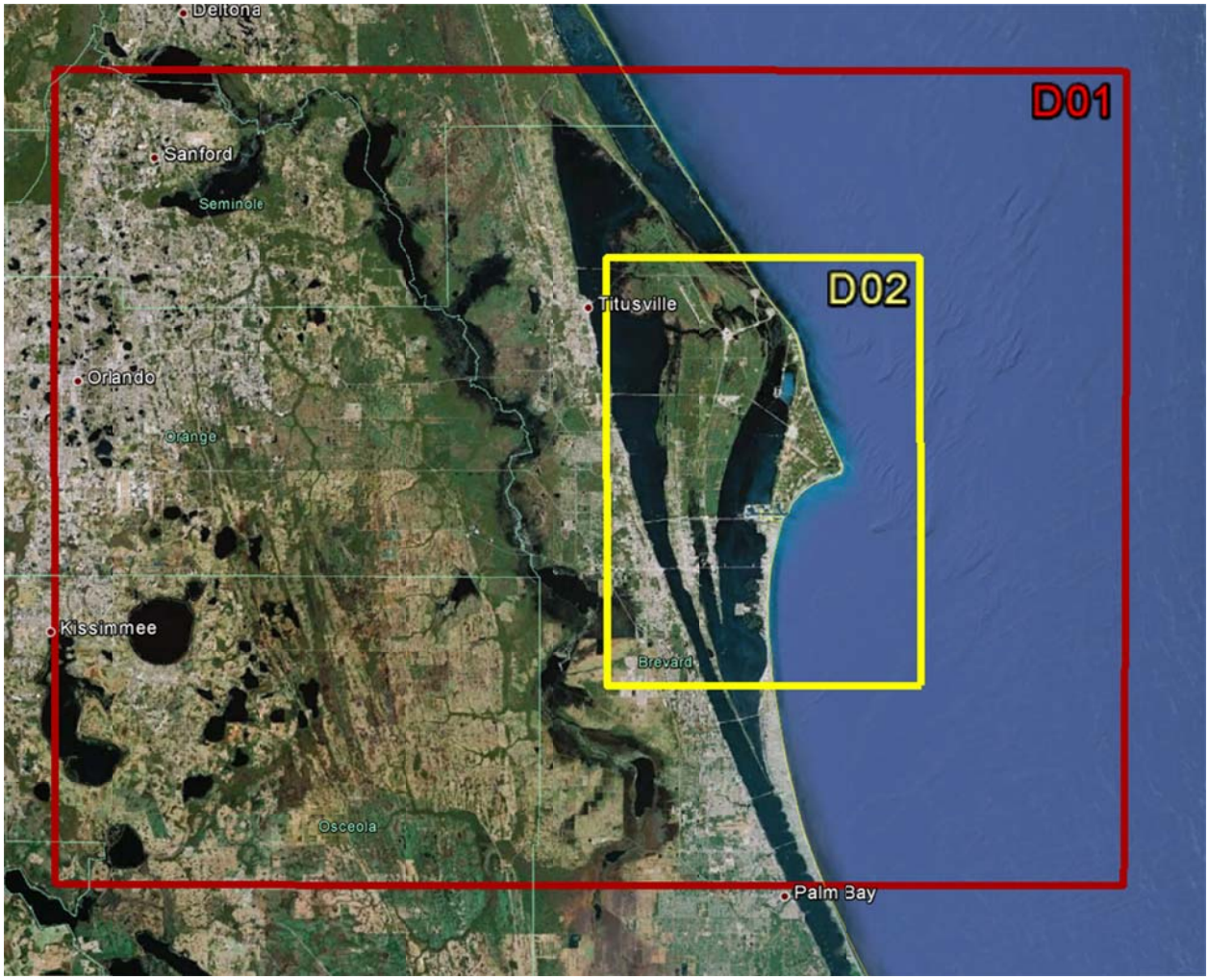

Figure 1. Map of east-central Florida showing the model domain boundaries. The red rectangle shows the outer domain and the yellow rectangle the inner domain for all configurations regardless of horizontal resolution or domain core.

2.2 Forecast Validation

The AMU validated the WRF model forecasts using simple statistics that compared locally available observational surface and upper air data to the forecast data. Precipitation forecasts were compared to nationally available rainfall data using a technique developed at NCAR. Two national models, the 13 km Rapid Update Cycle (RUC) and the 12 km NAM, were also validated against the same KSC/CCAFS wind towers in order to compare their performance to that of the WRF model surface forecasts.

2.2.1 Observed Data

Surface forecasts were validated with data from seven KSC/CCAFS wind towers, shown on the map in Figure 2. The model 10 m wind speed and direction and 2 m temperature (T) and dewpoint temperature (T_d) were validated with the 6 ft wind speed and direction and 54 ft T and T_d, respectively, from towers 2, 6, 108, 110, and 512. Model 10 m wind speed and direction were validated with 30 ft wind speed and direction from towers 511 and 513.

Upper air forecasts valid at 2200 UTC (7-hour forecast) for the warm season were validated with the daily 2200 UTC CCAFS (XMR) sounding (Figure 2). The model wind speed and direction, T, and T_d were compared to the observed values at 50 mb increments from 1000 mb to 100 mb.

Forecast accumulated rainfall was compared to the NCEP Stage-II (http://www.emc.ncep.noaa.gov/mmb/ylin/pcpanl/stage2/) analysis data to verify precipitation. This analysis is a national multi-sensor hourly precipitation analysis based on hourly radar precipitation estimates from the ~140 Level II Weather Surveillance Radar-1988 Doppler (WSR-88D) radars in the continental United States and ~3,000 automated gauge reports. The rainfall analysis provides hourly rainfall accumulation on a 4 km grid.

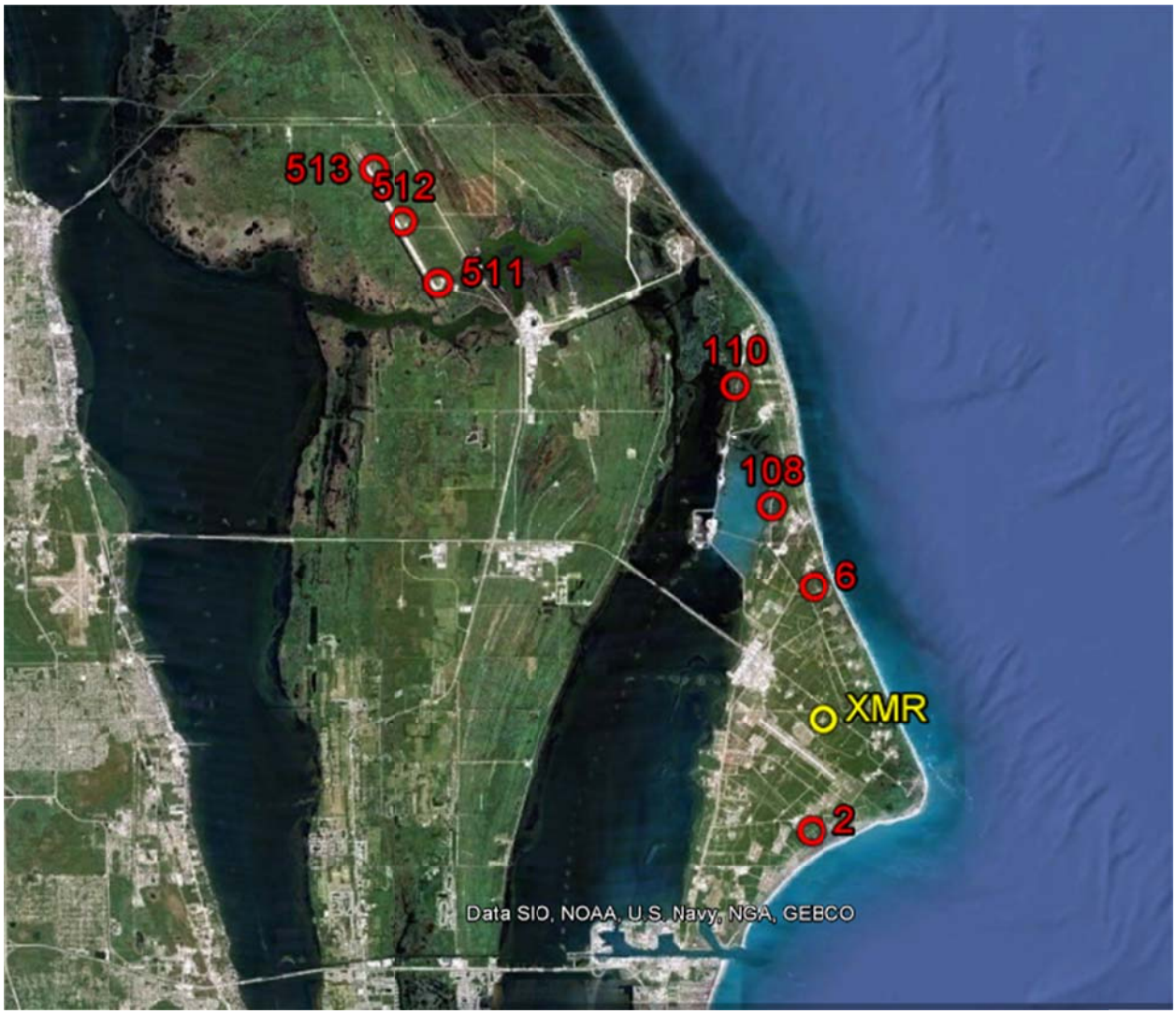

Figure 2. The locations of the seven KSC/CCAFS wind towers and their numbers that were used to validate the WRF forecasts on the ER are shown in red. The XMR RAOB site used to validate the upper air forecasts is shown in yellow.

2.2.2 Verification Statistics

The AMU calculated the same verification statistics for both the surface and upper air forecasts. The objective statistical analysis included the model bias, mean error (ME), and the root mean square error (RMSE). For the surface analysis, the observed wind speed and direction, T, and T_d were compared to the WRF forecast values output every 30 minutes. Statistics that evaluated the WRF model against the two national models compared the observations to the output data every 3 hours, which corresponds to the availability of the NAM model output. All statistics were computed using data from the inner WRF grids.

The model bias was calculated for each model forecast against every observation from each tower and the daily RAOB at each available level. This difference was calculated by subtracting the observed parameter from the model forecast as shown by the equation below.

$$\text{Diff}_{\text{WRF}} = \text{Model Forecast} - \text{Tower/RAOB Observation}$$

In order to make sense of the bias data, the ME was calculated for all tower and RAOB data during the period of interest. The ME is a measure of the overall bias of the model parameter being compared. A perfect forecast has ME = 0. It is defined as

$$ME = \frac{1}{n}\sum_{i=1}^{n}\left(f_i - o_i\right)$$

where:

n = number of model output times and/or vertical levels over the forecast period,

f_i = WRF forecast of T, T_d, wind speed, or wind direction (surface or upper air), and

o_i = observed T, T_d, wind speed, or wind direction (surface or upper air).

The model RMSE was calculated to measure the magnitude of the error. It is useful in determining whether the forecasts produced large errors, as it gives relatively high weight to large errors. It is calculated using the following equations:

$$MSE = \frac{1}{n}\sum_{i=1}^{n}(f_i - o_i)^2$$

$$RMSE = \sqrt{MSE}$$

where n, f_i, and o_i are defined as above.

To verify precipitation, rainfall accumulation throughout the entire forecast was compared to the observed rainfall over the same time period. MODE was used to determine the skill of each model configuration and it is available as part of the Model Evaluation Tools (MET) software that was developed by the NCAR Developmental Testbed Center (http://verif.rap.ucar.edu/eval/hwt/2011/spatial_eval.php). It is a state-of-the-art suite of verification tools that uses output from the WRF model to compute standard verification scores comparing gridded model data to point or gridded observations.

MODE is an object-based verification that compares gridded observations to gridded forecasts. It resolves and compares objects, such as areas of accumulated rainfall, in both the forecast and observed fields. The objects can be described geometrically and then the attributes of the objects can be compared (Davis et al. 2006). MODE outputs statistics that describe the correlation between the objects and allows the user to identify forecast strengths or weaknesses. Details about how objects are identified and characterized can be found in Davis et al. (2006). For this report, the objects of interest are areas of accumulated rainfall. Therefore,

references to ‘objects’ are references to areas of resolved accumulated rainfall throughout the forecast period.

Once the objects have been identified, their various properties are evaluated and compared. The object attributes examined by the AMU in this task included the centroid distance, area ratio, and total interest value. The centroid distance is the vector difference between the centroids of the forecast and observed objects. It describes the location bias in the forecasts. The smaller the distance between the centroids, the better the forecast. The area ratio compares the area, or number of grid squares, the forecast object occupies compared to the observed object. An area ratio of 1 is considered a perfect correlation. Interest value is defined as the differences in particular attributes between the forecast and observed objects. Interest values of 0 indicate no interest, or a poor forecast, while a value of 1 indicates high interest, or a good forecast. The total interest value is a weighted sum of specific interest values and is used as an overall indicator of the quality of the precipitation forecast. Total interest value is large when forecast and observed objects are well correlated (are roughly the same size and are close to each other) and is small when they are not well correlated.

2.3 Warm Season Results

Surface, upper air, and precipitation forecasts were compared to observations during part of the 2011 warm season. Different configurations of the WRF model were compared to determine if one configuration would consistently outperform the others.

2.3.1 Surface Forecasts

The AMU validated the WRF model forecasts with the KSC/CCAFS wind tower data. Two national models, the 13 km RUC and the 12 km NAM, were also validated against the same KSC/CCAFS wind towers for the month of August 2011 in order to compare their performance to that of the WRF model forecasts. Color-coded Good-Bad-Neutral (GBN) tables were populated with the computed ME and RMSE statistics. The tables are used to show which model configuration performed the best and worst. A good (green) rating indicates that the model configuration had the lowest ME or RMSE values among the different configurations. A bad (red) rating had the highest ME or RMSE values and neutral (yellow) fell in the middle.

Table 2 shows the GBN chart of the average 30-day ME for August 2011 between all seven wind towers and three WRF configurations and the two national models. The RUC model had the lowest ME for wind direction and T_d while the ARW configuration (Lin-YSU) had the lowest ME for wind speed and temperature. The AMU anticipated that the national models would outperform the WRF configurations since

- no observational data were assimilated into the WRF model,
- 3-hourly NAM forecasts were used for the WRF initial boundary conditions versus a 1-hourly forecast from the RUC since soil moisture and temperature data were not available in the archived RUC forecasts, and
- no high-resolution LIS or SST data were used since the AMU did not have the archive data.

Therefore it was surprising and encouraging to see the ARW configuration (Lin-YSU) perform so well. The national models were included in the comparison mainly to determine if the WRF forecasts were reasonable.

Table 2. GBN chart of the average 30-day ME for August 2011 for all seven KSC/CCAFS wind towers for the three initial WRF configurations and two national models.

30-day: Mean Error or Monthly Bias - All Towers				
Model	*Wind Dir (deg)*	*Wind Spd (m/s)*	*Temp (F)*	*Dewpt (F)*
12 km NAM	42.7	0.986	-0.240	-1.000
13 km RUC	37.9	0.814	-1.400	0.350
NMM 3/1	42.3	1.629	-0.660	-1.174
NMM 2/0.6	44.4	1.552	-0.713	-1.377
Lin-YSU	47.7	0.463	-0.236	-2.788

Of the three WRF forecasts run for August 2011, the only ARW configuration included in the initial comparison, Lin-YSU, produced the best wind speed and temperature forecasts, but the worst wind direction and T_d forecasts (Table 3). NMM 3/1 performed best for wind direction and T_d and worst for wind speed. NMM 2/0.6 fell somewhere in the middle for all forecasts except temperature. An RMSE value of 15.417 for temperature for NMM 2/0.6 indicates that there were large errors in some of the forecasts.

Table 3. GBN chart of the average 30-day ME and RMSE for 1-30 August 2011 for all seven KSC/CCAFS wind towers for the three initial WRF configurations.

30-day: Mean Error or Monthly Bias - All Towers				
Model	*Wind Dir (deg)*	*Wind Spd (m/s)*	*Temp (F)*	*Dewpt (F)*
NMM 3/1	42.3	1.629	-0.660	-1.174
NMM 2/0.6	44.4	1.552	-0.713	-1.377
Lin-YSU	47.7	0.463	-0.236	-2.788
30-day: RMSE - All Towers				
Model	*Wind Dir (deg)*	*Wind Spd (m/s)*	*Temp (F)*	*Dewpt (F)*
NMM 3/1	58.4	2.558	4.617	3.115
NMM 2/0.6	62.3	2.525	15.417	3.205
Lin-YSU	65.5	1.879	3.943	4.162

Table 4 gives the total number of good, bad, and neutral forecasts for the combined 30-day ME and RMSE of the three WRF configurations at the seven wind tower locations. Results indicate that Lin-YSU had the most 'good' forecasts followed closely by NMM 3/1.

Table 4. GBN totals from the ME and RMSE values for the three initial WRF configuration forecasts at the seven KSC/CCAFS wind towers during 1-30 August 2011.

1-30 August 2011 Totals			
Model	Good	Neutral	Bad
NMM 3/1	21	13	11
NMM 2/0.6	3	29	14
Lin-YSU	22	3	23

Based on these results and those of the precipitation and upper air comparison (detailed in Sections 2.3.2 and 2.3.3), the AMU decided to run seven more ARW configurations (Configurations 4-10) with different physics options, for a total of eight ARW runs, and compare the results. Due to time constraints, all configurations were run once per day at 1500 UTC from 1-7 August 2011 instead of for the whole month. In both ARW runs that used the GFS PBL scheme, the 2 m shelter temperatures routinely increased to unrealistic values of over 100 °F. Therefore, both Ferrier-GFS and WDM6-GFS (Configurations 9 and 10, respectively) were dropped from the comparison. Based on the 7-day ME for all towers (Table 5), both Lin-YSU and Ferrier-YSU outperformed the rest of the ARW model runs. Examining Table 6, Lin-YSU had the most 'good' forecasts and the least 'bad' forecasts, followed by Ferrier-YSU.

Table 5. GBN chart of the average ME and RMSE for 1-7 August 2011 for all seven KSC/CCAFS wind towers for the six ARW configurations.

7-day: Mean Error - All Towers				
Model	*Wind Dir (deg)*	*Wind Spd (m/s)*	*Temp (F)*	*Dewpt (F)*
Lin-YSU	47.3	-0.086	-0.900	-1.969
Ferrier-YSU	46.2	0.069	-1.064	-1.844
WDM6-YSU	50.3	0.009	-1.054	-2.323
Goddard-YSU	47.6	-0.023	-1.077	-1.952
Ferrier-MYJ	47.7	1.276	-0.955	-1.575
WDM6-MYJ	48.5	0.987	-0.597	-1.836
7-day: RMSE - All Towers				
Model	*Wind Dir (deg)*	*Wind Spd (m/s)*	*Temp (F)*	*Dewpt (F)*
Lin-YSU	63.1	1.400	2.369	3.224
Ferrier-YSU	62.6	1.403	2.432	3.010
WDM6-YSU	67.1	1.585	2.563	3.769
Goddard-YSU	63.6	1.497	2.364	3.117
Ferrier-MYJ	64.1	2.175	2.835	3.096
WDM6-MYJ	65.5	1.956	2.571	3.567

Table 6. GBN totals from the ME and RMSE values for the six ARW configuration forecasts at the seven KSC/CCAFS wind towers during 1-7 August 2011.

1-7 August 2011 Totals			
Model	Good	Neutral	Bad
Lin-YSU	13	32	1
Ferrier-YSU	12	32	2
WDM6-YSU	4	26	16
Goddard-YSU	4	41	1
Ferrier-MYJ	6	22	18
WDM6-MYJ	7	31	8

2.3.2 Upper Air Forecasts

The AMU validated the six ARW configurations against the daily 2200 UTC XMR sounding. Additional XMR sounding data are available at 1500 UTC in the warm season, however these data were not used in the comparison since the WRF forecasts were initialized at 1500 UTC. All model configurations had a similar 0-hour forecast and, therefore, the ME statistics between the observed and forecast values were essentially the same. The XMR sounding data was interpolated to match the model output that was available every 50 mb from 1000-100 mb. The average 7-day ME and RMSE were computed for wind direction, wind speed, T, and T_d (Table 7). Based on the results, Lin-YSU produced the best upper-air forecast followed by Ferrier-YSU.

Table 7. GBN chart of the average ME and RMSE for 1-7 August 2011 for the 2200 UTC XMR RAOB for the six ARW configurations.

7-day: Mean Error - XMR RAOB				
Model	*Wind Dir (deg)*	*Wind Spd (m/s)*	*Temp (F)*	*Dewpt (F)*
Lin-YSU	35.0	-0.146	0.436	-5.503
Ferrier-YSU	38.5	-0.046	0.387	-4.826
WDM6-YSU	37.7	0.159	0.491	-5.584
Goddard-YSU	35.9	-0.170	0.458	-5.631
Ferrier-MYJ	39.1	0.044	0.466	-5.345
WDM6-MYJ	35.1	-0.102	0.539	-6.761
7-day: RMSE - XMR RAOB				
Model	*Wind Dir (deg)*	*Wind Spd (m/s)*	*Temp (F)*	*Dewpt (F)*
Lin-YSU	50.2	2.542	1.785	15.381
Ferrier-YSU	54.5	2.545	1.818	15.970
WDM6-YSU	53.3	2.734	1.773	15.797
Goddard-YSU	50.5	2.611	1.826	15.591
Ferrier-MYJ	55.5	2.626	1.891	15.994
WDM6-MYJ	49.8	2.565	1.841	15.902

2.3.3 Precipitation Forecasts

The AMU compared precipitation forecasts from NMM 3/1, NMM 2/0.6, and Lin-YSU to determine performance differences between the NMM and ARW. The 9-hour forecast accumulated rainfall was compared to the 9-hour accumulation of observed rain using the NCEP Stage-II analysis data for each day from 1-30 August 2011. The monthly summary statistics of centroid distance, area ratio, and interest function from the MODE software are shown in Table 8. The centroid distance (km) results indicate that the Lin-YSU (ARW) precipitation matched the location of the observed precipitation most closely. An interest value of 0.92 indicates that overall the forecast correlates well with the observed precipitation. The area ratio for NMM 3/1 indicates that the forecast most closely matches the areal coverage of observed precipitation, followed by Lin-YSU. Overall, the ARW configuration outperformed both NMM configurations.

Table 8. GBN chart for the average 30-day MODE statistics for 1-30 August 2011 over the ER WRF domain for the initial three WRF configurations.

30-day: MODE - Precipitation Statistics			
Model	*Centroid Distance (km)*	*Area Ratio*	*Interest*
NMM 3/1	22.43	0.54	0.91
NMM 2/0.6	22.68	0.33	0.85
Lin-YSU	14.33	0.52	0.92

Based on these results, the same summary statistics were computed for the six additional ARW configurations for 1-7 August 2011 (Table 9). It is interesting to note that Ferrier-YSU produced the worst precipitation forecasts, but some of the best surface and upper air forecasts. In general, results indicate that the WDM6 microphysics option (WDM6-YSU and WDM6-MYJ) tended to produce the best precipitation forecasts. It should be noted that it took some time for precipitation to spin up in all model runs. Once observational data is assimilated, spin up time will decrease and individual performance of any model configuration may improve.

Table 9. GBN chart for the average MODE statistics for 1-7 August 2011 over the ER WRF domain for the six ARW configurations.

7-day: MODE – Precipitation Statistics			
Model	*Centroid Distance (km)*	*Area Ratio*	*Interest*
Lin-YSU	9.67	0.69	0.98
Ferrier-YSU	19.10	0.43	0.92
WDM6-YSU	16.36	0.79	0.98
Goddard-YSU	13.45	0.73	0.98
Ferrier-MYJ	9.60	0.58	0.97
WDM6-MYJ	13.45	0.72	0.99

2.4 Cool Season Results

Based on the warm season results, the AMU chose to compare the NMM 3/1, Lin-YSU, and Ferrier-YSU in the cool season. Both Lin-YSU and Ferrier-YSU performed consistently well, while NMM 3/1 was included as the better of the two NMM configurations (Table 8) to determine if the NMM performed better in the cool season. Test cases for the three configurations were

run for eight days from 18-25 February 2012. Two 9-hour forecasts were produced each day starting at 0000 and 1200 UTC using the 12 km NAM model for boundary and initial conditions, SPoRT LIS surface data, and SPoRT SST data.

2.4.1 Surface Variables

The AMU validated the WRF model forecasts with the KSC/CCAFS wind tower data from towers 2, 6, 108, and 110 as shown in Figure 2. Data for towers 511, 512, and 513 were not available between 18-25 February 2012. The two national models were also validated against the same KSC/CCAFS wind towers in order to compare their performance to that of the three WRF model forecasts. As in the warm season, Table 10 indicates that Lin-YSU had as many good forecasts for the ME and RMSE as the 13 km RUC. NMM 3/1 and the 12 km NAM performed the worst. In general, the cool season ME for wind direction, temperature, and dewpoint temperature were smaller than that for the warm season. Table 11 shows the 8-day GBN totals for ME and RMSE for all configurations and indicates that Lin-YSU had the most 'good' forecasts and outperformed all other configurations, including the 13 km RUC.

Table 10. GBN chart of the average ME and RMSE for 18-25 February 2012 for four KSC/CCAFS wind towers for the three initial WRF configurations and two national models.

8-day: Mean Error - All Towers				
Model	*Wind Dir (deg)*	*Wind Spd (m/s)*	*Temp (F)*	*Dewpt (F)*
NAM	29.5	0.409	0.487	0.875
RUC	29.0	0.890	0.338	1.387
NMM 3/1	29.5	1.154	0.764	0.693
Lin-YSU	29.7	-0.047	0.816	0.041
Ferrier-YSU	30.3	-0.039	0.769	0.053
8-day: RMSE - All Towers				
Model	*Wind Dir (deg)*	*Wind Spd (m/s)*	*Temp (F)*	*Dewpt (F)*
NAM	49.7	1.788	3.014	1.823
RUC	45.5	1.973	4.055	2.443
NMM 3/1	49.1	2.335	3.220	1.809
Lin-YSU	47.6	1.664	2.734	1.516
Ferrier-YSU	49.4	1.702	2.751	1.536

Table 11. GBN totals from the ME and RMSE values for the three initial WRF configurations and two national models at four KSC/CCAFS wind towers during 18-25 February 2012.

18-25 February 2012 Totals			
Model	Good	Neutral	Bad
NAM	6	21	3
RUC	8	11	11
NMM 3/1	2	17	11
Lin-YSU	11	15	4
Ferrier-YSU	3	26	1

2.4.2 Upper Air forecasts

XMR data were available at 1100 and 2300 UTC during the cool season. Since these times did not occur within the 9-hour 0000 or 1200 UTC forecast periods, the AMU could not compare the model output to the sounding data.

2.4.3 Precipitation forecasts

The AMU compared the 9-hour accumulation of observed rain using the NCEP Stage-II analysis data to the 9-hour forecast accumulated rainfall from the 0000 and 1200 UTC model runs for 18-25 February 2012. The summary statistics of centroid distance (km), area ratio, and interest function from the MODE software are shown in Table 12. The 'NA' designations for NMM 3/1 indicate that the model failed to forecast precipitation that matched the observations. The results indicate that Lin-YSU produced the best precipitation forecast, although it did not perform much better than Ferrier-YSU. The model did a better job of forecasting the warm season precipitation vs. the cold season precipitation. This can be explained by having less precipitation events in the cool season period of record and less rainfall during those events. In most cases the model did predict precipitation when it was observed, but forecast less precipitation than the observed events. In these cases, the forecast precipitation was filtered out due to the methods used by the MODE tool to resolve forecast and observed precipitation objects. The precipitation thresholds can be varied and were adjusted to account for the smaller rainfall amounts. However, even with the smaller thresholds the forecast precipitation was too light and was filtered out.

Table 12. GBN chart for the average MODE statistics for 18-25 February 2012 over the ER WRF domain.

8-Day: MODE - Precipitation Statistics			
Model	*Centroid Distance*	*Area Ratio*	*Interest*
NMM 3/1	NA	NA	NA
Lin-YSU	20.97	0.39	0.80
Ferrier-YSU	20.96	0.36	0.79

2.5 Additional Comparisons

The AMU compared three Lin-YSU configurations run once per day at 1500 UTC from 1-7 August 2011 with varying horizontal grid spacing to determine if a slightly coarser or finer resolution would have much impact on the results. The first configuration had a 2 km outer domain and a 0.67 km inner domain (Lin-YSU 2/0.6), the second had a 3 km outer and 1 km inner domain (Lin-YSU 3/1), and the third had a 1 km outer and 0.3 km inner domain (Lin-YSU 1/0.3). The ME and RMSE for wind direction, wind speed, T, and T_d were computed for each configuration at the seven KSC/CCAFS wind towers. Results are shown in Table 13. The results indicate that the two higher resolution model configurations slightly outperformed the coarser resolution for wind speed, T, and T_d. The Lin-YSU 3/1 outperformed the both the 2/0.67 and 1/0.3 configurations for wind direction.

Table 13. GBN chart of the average ME and RMSE for 1-7 August 2011for seven KSC/CCAFS wind towers for three ARW configurations with varying horizontal resolutions.

7-day: Mean Error - All Towers				
Model	*Wind Dir (deg)*	*Wind Spd (m/s)*	*Temp (F)*	*Dewpt (F)*
Lin-YSU (2/0.6)	47.4	-0.086	-0.880	-1.950
Lin-YSU (3/1)	43.0	0.143	-2.240	-1.950
Lin-YSU (1/0.3)	49.6	-0.097	-0.942	-1.879
7 day: RMSE - All Towers				
Model	*Wind Dir (deg)*	*Wind Spd (m/s)*	*Temp (F)*	*Dewpt (F)*
Lin-YSU (2/0.6)	63.1	1.400	2.369	3.224
Lin-YSU (3/1)	62.1	1.534	3.161	3.353
Lin-YSU (1/0.3)	65.9	1.335	2.632	3.039

2.6 Recommendations and Future Work

Warm and cool season results indicate that Lin-YSU is the optimal model configuration for the ER. It consistently produced the best surface and upper air forecasts, while performing fairly well for the precipitation forecasts. Therefore the AMU recommends running the WRF ARW over the ER using the Lin microphysical scheme and the YSU PBL scheme.

Running the model at a high horizontal resolution will require either a decrease in domain size or an increase in model run time. The user must ultimately decide if the higher resolution is worth the cost of the increase in computing resources or a decrease in domain size. The AMU recommends running the model with a 2 km outer and 0.67 km inner domain.

The next step in this study will be to provide a recommended local data assimilation (DA) and numerical forecast model design optimized for the ER to support space launch activities. The AMU will determine the best software and type of assimilation to use, as well as determine the best grid resolution for the initialization based on spatial and temporal availability of data and the wall clock run-time of the initialization. The AMU will also transition from the WRF EMS to the NASA Unified-WRF (NU-WRF), a NASA-specific version of the WRF that takes advantage of unique NASA software and datasets.

3. Wallops Flight Facility

This section describes the model configuration and test cases, results, and recommendations for an operational model for WFF.

3.1 Model Configuration and Test Cases

The most important part of this task was the model configuration. The users at WFF could benefit from an operational model that could offer them information that is not readily available from national models. This includes

- a higher resolution model that could run at a more frequent interval than the national models,
- a model that could output forecast data at a more frequent interval, and
- a model that could be configured for the unique weather patterns over the Delaware-Maryland-Virginia (Delmarva) Peninsula.

To meet these requirements, the AMU tested various WRF model configurations by varying the dynamical core, grid spacing, and domain size while running a 24-hour forecast. This enabled the AMU to present different grid configurations to WFF to allow them to choose the optimal configuration for their forecast needs.

The AMU conducted testing on a 6-year old local modeling cluster that consists of 24 nodes/48 processors. To estimate how the model would run on more modern equipment, the AMU scaled the model run-time information to that of a newer, faster cluster with similar specifications. The domain size or resolution may be further increased depending on the specifications of the cluster used to run the WRF model. In addition, the adaptive time-step option was turned on in the WRF model. The time-step length is a user-configurable parameter that normally remains constant throughout the model run. Choosing an appropriate time-step is important since one that is too long will cause instability and/or model failure and one that is too short is a waste of computing power. The adaptive time-step allows the time-step to be varied as necessary through the simulation to improve model performance and reduce the instability. Model run-time can be reduced using this option.

Personnel at WFF indicated that the optimal model configuration would allow for a 24-hour forecast and would include the entire Delmarva Peninsula. The AMU presented WFF with four configurations that varied in model core and domain size. WFF personnel chose a WRF ARW configuration with a 4 km outer and 1.33 km inner domain (Figure 3). The AMU decided to include an NMM configuration to test whether it produced a better forecast than the ARW (Figure 4). In addition, the AMU decided to run the ARW with different physics options and compare the results. The physics options were chosen based on the findings from the ER portion of the task (Section 2). Forecasts from the following four configurations[2], three ARW and one NMM, were compared:

Configuration 1: ARW core, 4 km outer domain and 1.33 km inner domain, Ferrier microphysics scheme, YSU PBL scheme (Ferrier-YSU),

Configuration 2: ARW core, 4 km outer domain and 1.33 km inner domain, Lin microphysics scheme, YSU PBL scheme (Lin-YSU),

Configuration 3: ARW core, 4 km outer domain and 1.33 km inner domain, WDM6 microphysics scheme, YSU PBL scheme (WDM6-YSU),

[2] Model configurations will be referenced by their name in parentheses in the results sections (3.3 and 3.4).

Configuration 4: NMM core, 3 km outer domain and 1 km inner domain, Ferrier microphysics scheme, MYJ PBL scheme (NMM 3/1).

All other physics parameters were the same for each ARW model run. The NMM runs did not use the same physics as the ARW runs since physics options are more limited for the NMM. Table 14 lists the physics options used in both the ARW and NMM runs that were held constant.

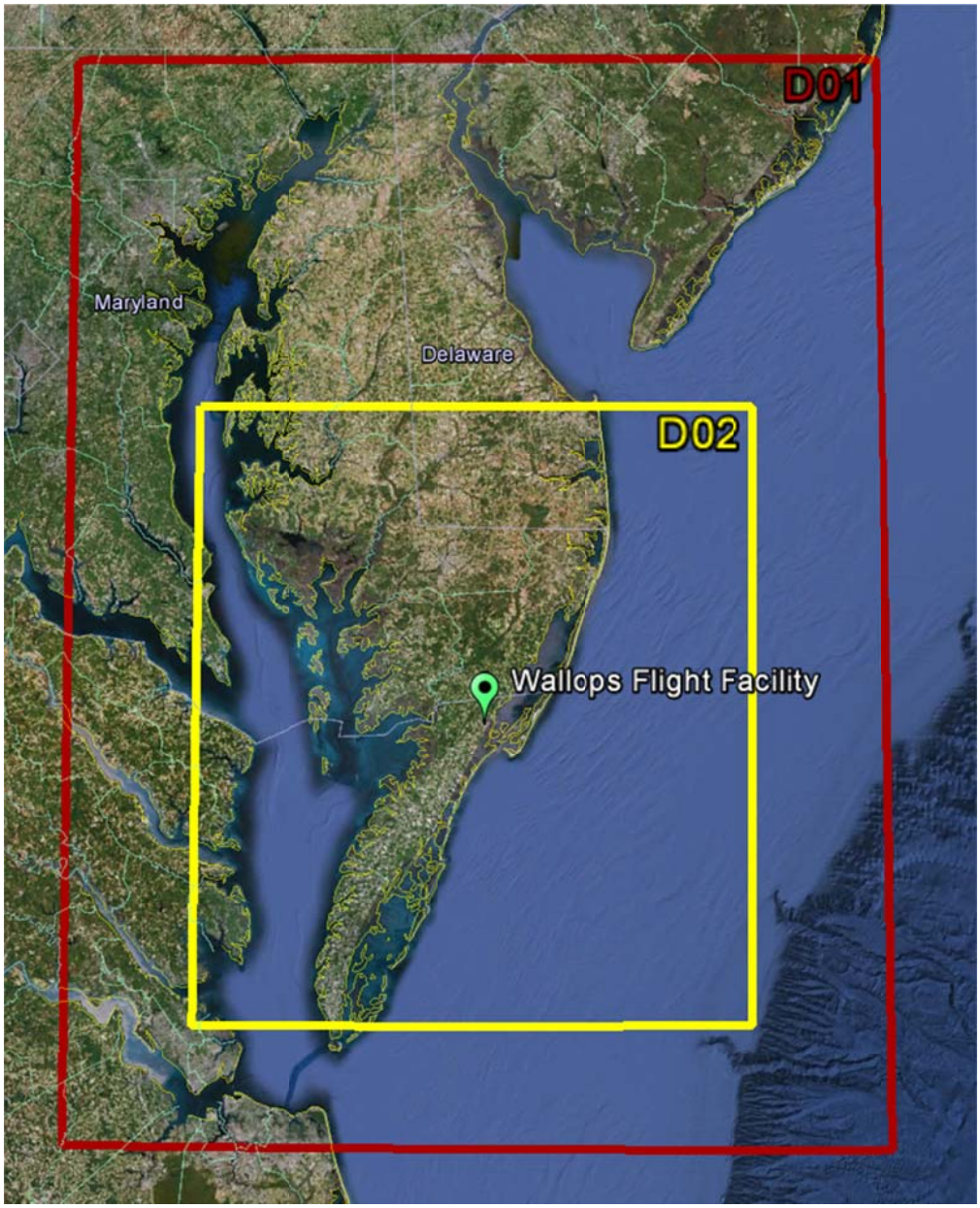

Figure 3. Map of the Delmarva Peninsula showing the WRF ARW model domain boundaries. The red rectangle shows the outer 4 km domain and the yellow rectangle the inner 1.33 km domain.

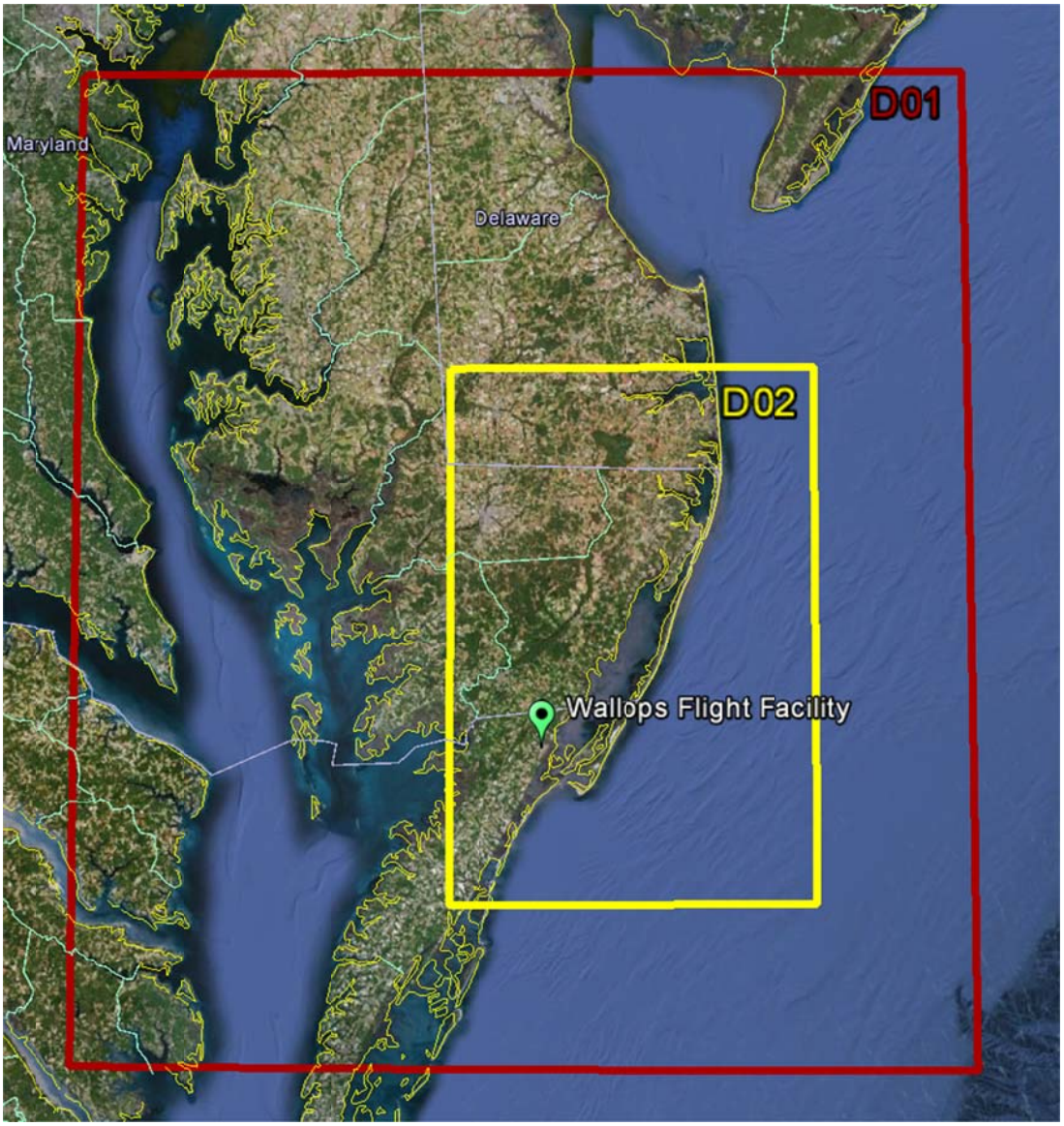

Figure 4. Map of the Delmarva Peninsula showing the WRF NMM model domain boundaries. The red rectangle shows the outer 3 km domain and the yellow rectangle the inner 1 km domain.

Table 14. List of additional physics options used for each model run for both the ARW and NMM cores.

Physics Option	ARW	NMM
Cumulus Parameterization	None	None
Land surface option	Noah Land Surface Model (Chen and Dudhia 2001)	Noah Land Surface Model (Chen and Dudhia 2001)
Shortwave radiation scheme	Dudhia (Dudhia 1989)	GFDL (Lacis and Hansen 1974)
Longwave radiation scheme	RRTM (Mlawer et al. 1997)	GFDL (Fels and Schwarzkopf 1975; Schwarzkopf and Fels 1985, 1991)

The AMU ran each model simulation at the specified horizontal resolution with 45 irregularly spaced, vertical sigma levels. Each run was integrated 24 hours twice per day and initialized at 0000 and 1200 UTC using the 12 km NAM model for boundary and initial conditions, SPoRT LIS surface data, and SPoRT SST data. Test cases for the ARW configurations were run from 1-14 November 2011 and 1-30 April 2012 to see if the model was able to accurately forecast the spring and fall season precipitation, temperature, and winds. An abbreviated set of test cases were run for the NMM configuration since the AMU had determined that the ARW performed better than the NMM in the ER portion of the task (Section 2). Test cases for the NMM were run from 1-7 November 2011.

3.2 Forecast Validation

The AMU validated the WRF model forecasts using simple statistics that compared locally available observational surface and upper air data to the forecast data. Precipitation forecasts were compared to nationally available rainfall data using a technique developed at NCAR. The 12 km NAM was also validated against the same observational data in order to compare its performance to that of the WRF model surface forecasts. The 13 km RUC was not evaluated because archive RUC forecast data is only available out to 12 hours.

3.2.1 Observed Data

Surface forecasts from the ARW runs were validated with data from seven METAR stations and four weather buoys located within the domain of interest. Figure 5 shows the seven METAR sites in red and four buoy locations in green. The model 10 m wind speed and direction and 2 m T and T_d were validated with the observed surface wind speed and direction, T, and T_d. For comparisons that involved the NMM model, surface forecasts were validated with data from three METAR sites (KWAL, KOXB, and KSBY) since those sites were the only ones that fell within the NMM inner domain.

Upper air forecasts for the 0000 UTC initialized runs valid at 1200 and 0000 UTC (12- and 24-hour forecasts) were validated with the daily 1200 and 0000 UTC sounding taken at KWAL (Figure 5). Upper air forecasts for the 1200 UTC initialized runs valid at 0000 and 1200 UTC (12- and 24-hour forecasts) were validated with the daily 0000 and 1200 UTC KWAL sounding. The model wind speed and direction, T, and T_d were compared to the observed values at 10 vertical levels: 1000, 850, 700, 500, 400, 300, 250, 200, 150, and 100 mb.

Forecast accumulated rainfall was compared to the NCEP Stage-II analysis data to verify precipitation. This analysis is a national multi-sensor hourly precipitation analysis based on hourly radar precipitation estimates from the ~140 WSR-88D radars in the continental United States and ~3,000 automated gauge reports. The rainfall analysis provides hourly rainfall accumulation on a 4 km grid.

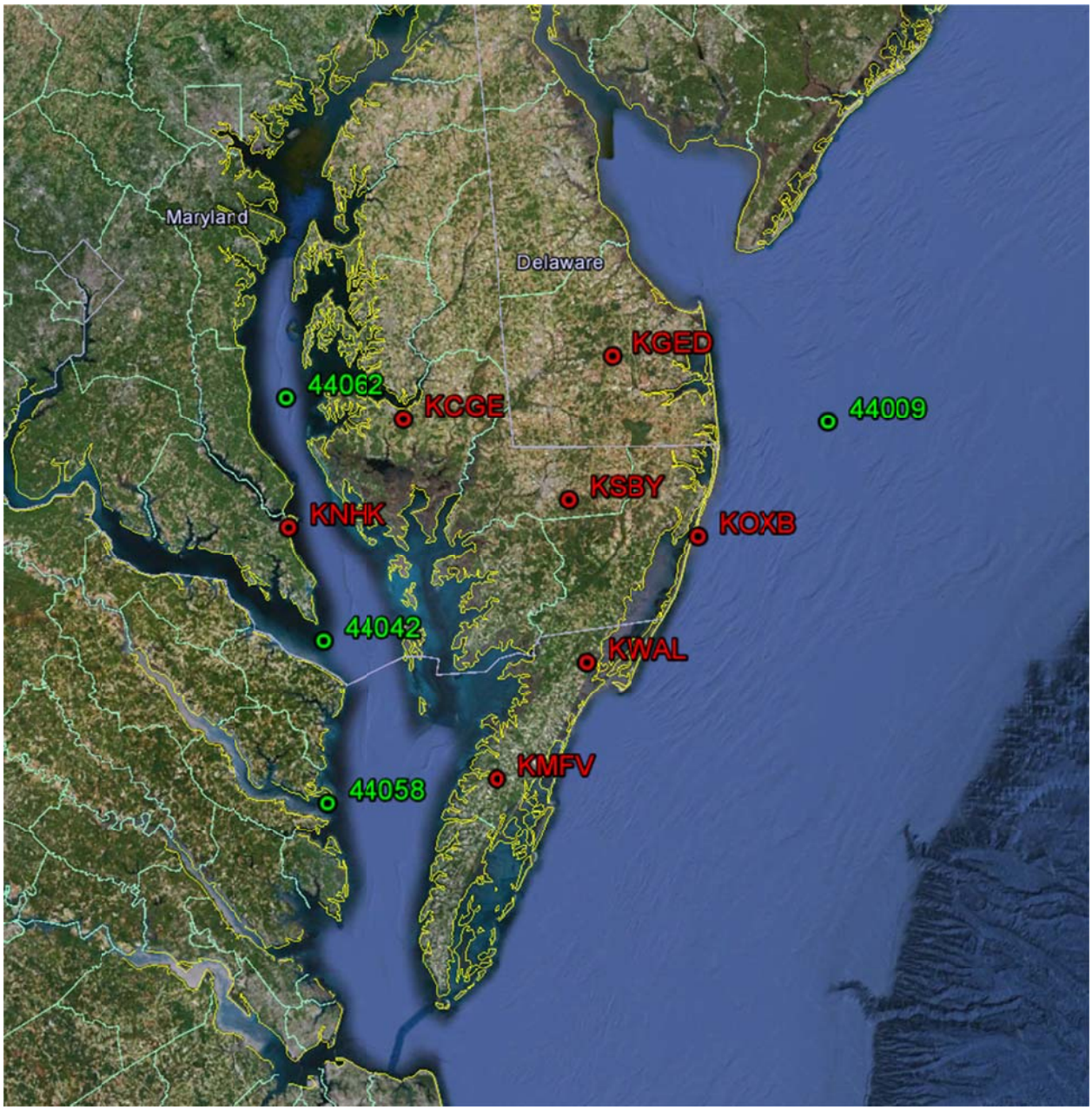

Figure 5. Seven METAR (red) and four buoy (green) weather reporting stations that were used to validate the WRF forecasts for WFF. The sounding was taken at the KWAL location.

3.2.2 Verification Statistics

The AMU calculated the same verification statistics for both the surface an upper air forecasts. The objective statistical analysis included the model bias, ME, and the RMSE. For the surface analysis, the observed wind speed and direction, T, and T_d were compared to the WRF

forecast values output every 60 minutes. Statistics that evaluated the WRF model against the two national models compared the observations to the output data every 3 hours, which corresponds to the availability of the NAM model output. All statistics were computed using data from the inner WRF grids.

The model bias was calculated for each model forecast against every observation from each METAR and buoy report, and the daily RAOB at each available level. This difference was calculated by subtracting the observed parameter from the model forecast as shown by the equation below.

$$\text{Diff}_{\text{WRF}} = \text{Model Forecast} - \text{METAR/RAOB Observation}$$

In order to make sense of the bias data, the ME was calculated for each METAR, buoy and the RAOB observation for the period of interest. The ME is a measure of the overall bias of the model parameter being compared. A perfect forecast has ME = 0. It is defined as:

$$ME = \frac{1}{n}\sum_{i=1}^{n}\left(f_i - o_i\right)$$

where:

n = number of model output times and/or vertical levels over the forecast period,

f_i = WRF forecast of T, T_d, wind speed, or wind direction (surface or upper air), and

o_i = observed T, T_d, wind speed, or wind direction (surface or upper air).

The model RMSE was calculated to measure the magnitude of the error. It is useful in determining whether the forecasts produced large errors, as it gives relatively high weight to large errors. It is calculated using the following equations:

$$MSE = \frac{1}{n}\sum_{i=1}^{n}(f_i - o_i)^2$$

$$RMSE = \sqrt{MSE}$$

where n, f_i, and o_i are defined as above.

To verify precipitation, rainfall accumulation throughout the entire forecast was compared to the observed rainfall over the same time period. MODE was used to determine the skill of each model configuration. MODE is available as part of the MET software that was developed by the NCAR Developmental Testbed Center (http://verif.rap.ucar.edu/eval/hwt/2011/spatial_eval.php). It is a state-of-the-art suite of verification tools that uses output from the WRF model to compute standard verification scores comparing gridded model data to point or gridded observations.

MODE is an object-based verification that compares gridded observations to gridded forecasts. It resolves and compares objects, such as areas of accumulated rainfall, in both the forecast and observed fields. The objects can be described geometrically and then the attributes of the objects can be compared (Davis et al. 2005). MODE outputs statistics that describe the correlation between the objects and allows the user to identify forecast strengths or weaknesses. Details about how objects are identified and characterized can be found in Davis et al. (2005). For this report, the objects of interest are areas of accumulated rainfall. Therefore, references to ‘objects’ are references to areas of resolved accumulated rainfall throughout the forecast period.

Once the objects have been identified, their various properties are evaluated and compared. The object attributes examined by the AMU in this task included the centroid distance, area

ratio, and total interest value. The centroid distance is the vector difference between the centroids of the forecast and observed objects. It describes the location bias in the forecasts. The smaller the distance between the centroids, the better the forecast. The area ratio compares the area, or number of grid squares, the forecast object occupies compared to the observed object. An area ratio of 1 is considered a perfect correlation. Interest value is defined as the differences in particular attributes between the forecast and observed objects. Interest values of 0 indicate no interest, or a poor forecast, while a value of 1 indicates high interest, or a good forecast. The total interest value is a weighted sum of specific interest values and is used as an overall indicator of the quality of the precipitation forecast. Total interest value is large when forecast and observed objects are well correlated (are roughly the same size and are close to each other) and is small when they are not well correlated.

3.3 Fall Season Results

The AMU compared the surface, upper air, and precipitation forecasts to observations during part of the 2011 fall season. Different configurations of the WRF model were compared to determine if one configuration would consistently outperform the others. Test cases involving the national model and the NMM configuration were run for seven days from 1-7 November 2011. Test cases that compared the ARW configurations were run for 14 days from 1-14 November 2011. The AMU produced two 24-hour forecasts each day starting at 0000 and 1200 UTC using the 12 km NAM model for boundary and initial conditions, SPoRT LIS surface data, and SPoRT SST data.

3.3.1 Surface Forecasts

The AMU validated the WRF model forecasts with the local METAR data. The 12 km NAM was also validated against the same METAR data for the first week of November 2011 in order to compare its performance to that of the WRF model forecasts. Color-coded GBN tables were populated with the computed ME and RMSE statistics. The tables are used to show which model configuration performed the best and worst. A good (green) rating indicates that the model configuration had the lowest ME or RMSE values among the different configurations. A bad (red) rating had the highest ME or RMSE values and neutral (yellow) fell in the middle.

Table 15 shows the GBN chart of the average 7-day ME and RMSE for 1-7 November 2011 between three METAR sites and four WRF configurations and one national model. The results were varied. The good forecasts outperformed the neutral forecasts only marginally. However, the bad forecasts were considerably worse than the good/neutral forecasts. In order to compare the forecasts it may be prudent to look at the lowest number of bad forecasts rather than focusing on the highest number of good forecasts. In this case, NMM 3/1 performed the worst followed by Lin-YSU and WDM6-YSU. The 12 km NAM fell somewhere in the middle while Ferrier-YSU marginally outperformed the rest of the configurations. The AMU anticipated that the national model would outperform the WRF configurations since no observational data was assimilated into the WRF model. Therefore it was surprising and encouraging to see the WRF configurations perform so well. The national model was included in the comparison mainly to determine if the WRF forecasts were reasonable.

Table 16 gives the total number of good, bad, and neutral forecasts for the 7-day combined ME and RMSE of the three METAR sites for all WRF configurations. Focusing on minimizing the bad forecasts, Ferrier-YSU produced the least bad forecasts. The NAM model and NMM 3/1 produced the most ‘good’ forecasts, but also had a fairly large number of ‘bad’ forecasts.

Table 15. GBN chart of the average 7-day ME and RMSE for 1-7 November 2011 for three METAR sites for four WRF configurations and one national model.

7 day: Mean Error - 3 METAR Sites				
Model	*Wind Dir (deg)*	*Wind Spd (m/s)*	*Temp (F)*	*Dewpt (F)*
Ferrier-YSU	30.54	1.076	-1.660	-0.819
Lin-YSU	30.44	1.039	-1.791	-0.857
WDM6-YSU	31.19	1.104	-1.592	-0.791
NMM 3/1	24.78	2.013	2.545	1.773
12 km NAM	26.98	1.263	1.954	2.265
7 day: RMSE - 3 METAR Sites				
Model	*Wind Dir (deg)*	*Wind Spd (m/s)*	*Temp (F)*	*Dewpt (F)*
Ferrier-YSU	44.34	1.976	4.113	3.111
Lin-YSU	44.67	2.036	4.220	3.017
WDM6-YSU	44.54	2.062	4.071	3.121
NMM 3/1	35.70	2.818	3.893	2.812
12 km NAM	39.47	2.017	3.312	3.100

Table 16. GBN totals from the ME and RMSE values for the four WRF and one national model forecasts at the three METAR sites during 1-7 November 2011.

1-7 November 2011 Totals			
Model	Good	Neutral	Bad
Ferrier-YSU	3	20	1
Lin-YSU	2	18	4
WDM6-YSU	4	15	5
NMM 3/1	7	7	9
12 km NAM	8	11	5

The AMU ran an additional seven days in November 2011 for each of the three ARW configurations and compared the results from 1-14 November 2011. Table 17 shows the GBN chart of the average 14-day ME and RMSE for 1-14 November 2011 between all seven METAR and four buoy sites and the three ARW configurations. The chart indicates that Lin-YSU performed the best, however the difference in ME and RMSE values between all configurations is fairly negligible. Examining Table 18, Ferrier-YSU had the most ‘good’ forecasts and the least ‘bad’ forecasts, while Lin-YSU had the most ‘bad’ forecasts. These results seem to conflict with those from Table 17, but can be explained by the negligible differences in forecast statistics for all ARW runs.

Table 17. GBN chart of the average ME and RMSE for 1-14 November 2011 for all seven METAR and four buoy sites for three ARW configurations.

14-day: Mean Error - All METAR/Buoy Sites				
Model	*Wind Dir (deg)*	*Wind Spd (m/s)*	*Temp (F)*	*Dewpt (F)*
Ferrier-YSU	27.9	0.778	-2.651	-0.631
Lin-YSU	27.6	0.738	-2.631	-0.666
WDM6-YSU	28.9	0.761	-2.503	-0.681
14-day: RMSE - All METAR/Buoy Sites				
Model	*Wind Dir (deg)*	*Wind Spd (m/s)*	*Temp (F)*	*Dewpt (F)*
Ferrier-YSU	40.1	2.122	4.354	3.073
Lin-YSU	39.8	2.168	4.542	3.173
WDM6-YSU	42.1	2.127	4.360	3.044

Table 18. GBN totals from the ME and RMSE values for the three ARW forecasts at all seven METAR and four buoy sites during 1-14 November 2011.

1-14 November 2011 Totals			
Model	Good	Neutral	Bad
Ferrier-YSU	26	15	15
Lin-YSU	18	13	25
WDM6-YSU	12	28	16

3.3.2 Upper Air Forecasts

The AMU validated the three ARW configurations against the daily 0000 and 1200 UTC KWAL sounding. Twelve and 24-hour upper air forecasts for the 0000 and 1200 UTC initialized runs were validated with the corresponding KWAL sounding. The AMU used 10 vertical levels in the KWAL sounding for validation: 1000, 850, 700, 500, 400, 300, 250, 200, 150, and 100 mb. The average 14-day ME and RMSE were computed for wind direction, wind speed, T, and T_d (Table 19). Based on the results, WDM6-YSU produced the best upper-air forecast followed by Lin-YSU. Again, differences in the computed statistics were small with the exception of T_d.

Table 19. GBN chart of the average ME and RMSE for 1-14 November 2011 for the 0000 and 1200 UTC KWAL RAOB and the three ARW configurations.

14-day: Mean Error - KWAL ROAB				
Model	*Wind Dir (deg)*	*Wind Spd (m/s)*	*Temp (F)*	*Dewpt (F)*
Ferrier-YSU	10.87	-0.866	-0.076	2.808
Lin-YSU	10.73	-0.869	-0.063	-0.015
WDM6-YSU	10.62	-0.861	-0.083	2.812
14-day: RMSE - KWAL RAOB				
Model	*Wind Dir (deg)*	*Wind Spd (m/s)*	*Temp (F)*	*Dewpt (F)*
Ferrier-YSU	18.91	2.558	2.105	9.788
Lin-YSU	18.71	2.549	2.106	0.744
WDM6-YSU	18.52	2.533	2.081	9.796

3.3.3 Precipitation Forecasts

The AMU compared precipitation forecasts from the three ARW configurations to determine which produced the best forecast. The 24-hour forecast accumulated rainfall was compared to the 24-hour accumulation of observed rain using the NCEP Stage-II analysis data for each day from 1-14 November 2011. The summary statistics of centroid distance, area ratio, and interest function from the MODE software are shown in Table 20. The centroid distance (km) results indicate that the Lin-YSU precipitation matched the location of the observed precipitation most closely. An interest value of 0.99 indicates that overall the Lin-YSU forecast correlates well with the observed precipitation. The area ratio for WDM6-YSU indicates that the forecast most closely matches the areal coverage of observed precipitation, followed by Ferrier-YSU. Lin-YSU performed worst in areal coverage of precipitation, but overall it outperformed the other configurations. It should be noted that during the 14 days there were not many precipitation events and there was little rainfall during those events. In most cases either the observed or forecast precipitation was filtered out due to the methods used by the MODE tool to resolve forecast and observed precipitation objects. The precipitation thresholds can be varied and were adjusted to account for the smaller rainfall amounts. However, even with the smaller thresholds the forecast precipitation was too light and was filtered out. In addition, once observational data is assimilated, individual performance of any model configuration may improve.

Table 20. GBN chart for the average 14-day MODE statistics for 1-14 November 2011 over the WFF WRF domain for the three ARW configurations.

14-day: MODE - Precipitation Statistics			
Model	*Centroid Distance (km)*	*Area Ratio*	*Interest*
Ferrier-YSU	8.59	0.97	0.98
Lin-YSU	3.02	0.88	0.99
WDM6-YSU	8.82	0.98	0.98

3.4 Spring Season Results

Based on the fall season results, the AMU chose to compare the ARW configurations in the spring season. The NMM configuration was dropped from the comparison since it was only

included to determine if it produced a superior forecast, which it did not. Test cases for the three configurations were run for 30 days from 1-30 April 2012. Two 24-hour forecasts were produced each day starting at 0000 and 1200 UTC using the 12 km NAM model for boundary and initial conditions, SPoRT LIS surface data, and SPoRT SST data.

3.4.1 Surface Variables

The AMU validated the WRF model forecasts with the local METAR and buoy data for the month of April 2012. Table 21 shows the GBN chart of the average 30-day ME and RMSE for all three configurations. It indicates that differences in statistics for all configurations were negligible as in the fall season. Lin-YSU performed the best, followed by Ferrier-YSU. Table 22 shows the total number of good, bad, and neutral forecasts for the 30-day combined ME and RMSE at the METAR and buoy sites. The results are consistent and show Lin-YSU performing the best followed by Ferrier-YSU. WDM6-YSU consistently performed the worst.

Table 21. GBN chart of the average 30-day ME for 1-30 April 2012 for all seven METAR and four buoy sites for three ARW configurations.

30-day: Mean Error or Monthly Bias - All METAR/Buoy Sites				
Model	*Wind Dir (deg)*	*Wind Spd (m/s)*	*Temp (F)*	*Dewpt (F)*
Ferrier-YSU	26.68	1.081	-0.222	-0.043
Lin-YSU	25.9	1.123	-0.101	1.575
WDM6-YSU	26.70	1.099	-0.148	0.013
30-day: RMSE - All METAR/Buoy Sites				
Model	*Wind Dir (deg)*	*Wind Spd (m/s)*	*Temp (F)*	*Dewpt (F)*
Ferrier-YSU	38.9	2.2746	2.260	1.539
Lin-YSU	37.5	2.2753	1.967	1.527
WDM6-YSU	38.5	2.305	2.261	1.551

Table 22. GBN totals from the ME and RMSE values for the three ARW forecasts at the seven METAR and four buoy sites during 1-30 April 2012.

1-30 April 2012 Totals			
Model	Good	Neutral	Bad
Ferrier-YSU	27	29	23
Lin-YSU	45	13	22
WDM6-YSU	9	35	36

3.4.2 Upper Air forecasts

The AMU validated the three ARW configurations against the daily 0000 and 1200 UTC KWAL sounding. As with the fall forecasts, 12- and 24-hour upper air forecasts for the 0000 and 1200 UTC initialized runs were validated with the corresponding KWAL sounding. The data were validated with the same vertical levels as in the fall forecasts. The average 30-day ME and RMSE were computed for wind direction, wind speed, T, and T_d (Table 23). Based on the

results, Lin-YSU produced the best upper-air forecast followed by WDM6-YSU. Again, differences in the computed statistics were small with the exception of T_d.

Table 23. GBN chart of the average ME and RMSE for 1-30 April 2012 for the 0000 and 1200 UTC KWAL RAOB for the three ARW configurations.

30-day: Mean Error - KWAL RAOB				
Model	*Wind Dir (deg)*	*Wind Spd (m/s)*	*Temp (F)*	*Dewpt (F)*
Ferrier-YSU	9.58	0.052	-0.490	3.474
Lin-YSU	9.51	0.030	-0.479	-0.026
WDM6-YSU	9.46	0.046	-0.483	3.287
30-day: RMSE - KWAL RAOB				
Model	*Wind Dir (deg)*	*Wind Spd (m/s)*	*Temp (F)*	*Dewpt (F)*
Ferrier-YSU	14.68	3.358	3.071	10.026
Lin-YSU	14.45	3.416	3.103	0.563
WDM6-YSU	14.25	3.428	3.144	10.030

3.4.3 Precipitation forecasts

The AMU compared the 24-hour accumulation of observed rain using the NCEP Stage-II analysis data to the 24-hr forecast accumulated rainfall from the 0000 and 1200 UTC model runs from 1-30 April 2012. The summary statistics of centroid distance (km), area ratio, and interest function from the MODE software are shown in Table 24. The results indicate that WDM6-YSU produced the best precipitation forecast, while Lin-YSU performed the worst. The Lin-YSU model did a better job of forecasting the fall season precipitation vs. the spring season precipitation. Since there were twice as many forecasts run in the spring season, more precipitation events were captured in the spring than in the fall. Therefore, it is more likely that the spring statistics are a more accurate representation of the skill of the model in predicting accumulated rainfall. In addition, once observational data is assimilated, individual performance of any model configuration may improve.

Table 24. GBN chart for the average 30-day MODE statistics for 1-30 April 2012 over the WFF WRF domain.

30-day: MODE - Precipitation Statistics			
Model	*Centroid Distance (km)*	*Area Ratio*	*Interest*
Ferrier-YSU	12.37	0.75	0.93
Lin-YSU	16.01	0.69	0.88
WDM6-YSU	10.85	0.80	0.92

3.5 Recommendations and Future Work

Fall and spring season results indicate that while all three ARW configurations performed similarly, both Ferrier-YSU and Lin-YSU performed slightly better than WDM6-YSU and better than the NMM configuration. Therefore, either Ferrier-YSU or Lin-YSU is the optimal model configuration for WFF. The AMU recommends running the WRF ARW over WFF using either

the Lin or Ferrier microphysical scheme and the YSU PBL scheme with a 4 km outer domain and a 1.33 km inner domain.

The next step in this study will be to provide a recommended local DA and numerical forecast model design optimized for WFF to support space launch activities. The AMU will determine the best software and type of assimilation to use, as well as determine the best grid resolution for the initialization based on spatial and temporal availability of data and the wall clock run-time of the initialization. The AMU will transition from the WRF EMS to NU-WRF, a NASA-specific version of the WRF that takes advantage of unique NASA software and datasets.

4. Summary and Future Work

This report summarizes the findings from an AMU task to determine the best model configuration for operational use at the ER and WFF to best predict winds, precipitation, and temperature. The AMU ran test cases in the warm and cool seasons at the ER and for the spring and fall seasons at WFF. For both the ER and WFF, the ARW core outperformed the NMM core. Results for the ER indicate that the Lin microphysical scheme and the YSU PBL scheme is the optimal model configuration for the ER. It consistently produced the best surface and upper air forecasts, while performing fairly well for the precipitation forecasts. Both the Ferrier and Lin microphysical schemes in combination with the YSU PBL scheme performed well for WFF in the spring and fall seasons.

The AMU has been tasked with a follow-on modeling effort to recommended local DA and numerical forecast model design optimized for both the ER and WFF to support space launch activities. The AMU will determine the best software and type of assimilation to use, as well as determine the best grid resolution for the initialization based on spatial and temporal availability of data and the wall clock run-time of the initialization. The AMU will transition from the WRF EMS to NU-WRF, a NASA-specific version of the WRF that takes advantage of unique NASA software and datasets.

References

Chen, F., and J. Dudhia, 2001: Coupling an advanced land-surface/ hydrology model with the Penn State/ NCAR MM5 modeling system. Part I: Model description and implementation. *Mon. Wea. Rev.*, **129**, 569–585.

Chen, S. H., and W. Y. Sun, 2002: A one-dimensional time dependent cloud model. *J. Meteor. Soc. Japan,* **80,** 99–118.

Cheng, W., Y. Liu, Y. Zhang, Y. Liu, D. Rostkier-Edelstein, A. Piterkovski, B. Mahoney, T. Warner, S. Drobot, 2010: Sensitivity of WRF-RTFDDA model physics in weather forecasting applications: From synoptic scale to meso-gamma scale. *11th Annual WRF Users' Workshop*. NCAR/RAL, Boulder, CO.

Davis, C., B. Brown, and R. Bullock, 2006: Object-based verification of precipitation forecasts. Part I: Methods and application to mesoscale rain areas. *Mon. Wea. Rev.*, **134,** 1772–1784.

Dudhia, J., 1989: Numerical study of convection observed during the Winter Monsoon Experiment using a mesoscale two-dimensional model. *J. Atmos. Sci.,* **46**, 3077–3107.

Fels, S. B., and M. D. Schwarzkopf, 1975: The simplified exchange approximation: A new method for radiative transfer calculations. *J. Atmos. Sci*., **32**, 1475-1488.

Gallus, W. A. and J. F. Bresch, 2006: Comparison of impacts of WRF dynamic core, physics package, and initial conditions on warm season rainfall forecasts, *Mon. Wea. Rev.*, **134**, 2632–2641.

Holt, T. and S. Raman. 1988. A review and comparative evaluation of multilevel boundary layer parameterizations for first-order and turbulent kinetic energy closure schemes. *Rev. Geophys.*, **26**, 761–780.

Hong, S. Y. and H. L. Pan, 1996: Non-local boundary layer vertical diffusion in a medium-range forecast model. *Mon. Wea. Rev.*, **124**, 2322-2339.

Hu, X. U., J. W. Nielsen-Gammon, and F. Zhang, 2010: Evaluation of three planetary boundary layer schemes in the WRF model. *J. Climate Appl. Meteor.*, **49**, 1831-1844.

Janjic, Z. I., 1984: Non–linear advection schemes and energy cascade on semi–staggered grids. *Mon. Wea. Rev*, **112**, 1234–1245.

Janjic, Z. I., 1990: The step-mountain coordinate: physical package, *Mon. Wea. Rev.*, **118**, 1429–1443.

Janjic, Z. I., 1996: The surface layer in the NCEP Eta Model. *Eleventh Conference on Numerical Weather Prediction*, Norfolk, VA, 19–23 August, Amer. Meteor. Soc., Boston, MA, 354–355.

Janjic, Z. I., 2002: Nonsingular Implementation of the Mellor–Yamada Level 2.5 Scheme in the NCEP Meso model, NCEP Office Note, No. 437, 61 pp.

Janjic, Z. I., 2003a: A nonhydrostatic model based on a new approach. *Meteor. Atmos. Phys.,* **82**, 271-285.

Janjic, Z. I., 2003b: The NCEP WRF core and further development of its physical package. *5th Int. SRNWP Workshop on Non-Hydrostatic Modeling,* Bad Orb, Germany, 27-29 October.

Janjic, Z. I., J. P. Gerrity Jr., and S. Nickovic, 2001: An alternative approach to nonhydrostatic modeling. *Mon. Wea. Rev.*, **129**, 1164-1178.

Jankov, I., W. A., Gallus, M., Segal, B., Shaw, and S. E., Koch, 2005: The impact of different WRF model physical parameterizations and their interactions on warm season MCS rainfall. *Wea. Forecasting*, **20**, 1048-1060.

Lacis, A. A., and J. E. Hansen, 1974: A parameterization for the absorption of solar radiation in the earth's atmosphere. *J. Atmos. Sci.*, **31**, 118–133.

Lim, K. S. and S. Y. Hong, 2010: Development of an effective double-moment cloud Microphysics scheme with prognostic cloud condensation nuclei (CCN) for weather and climate models. *Mon. Wea. Rev.*, **138**, 1587–1612.

Lin, Y. L., R. D. Farley, and H. D. Orville, 1983: Bulk parameterization of the snow field in a cloud model. *J. Climate Appl. Meteor.*, **22**, 1065–1092.

Mellor, G. L. and T. Yamada, 1982: Development of a turbulence closure model for geophysical fluid problems. *Rev. Geophys.*, **20**, 851–875.

Mlawer, E. J., S. J. Taubman, P. D. Brown, M. J. Iacono, and S. A. Clough, 1997: Radiative transfer for inhomogeneous atmosphere: RRTM, a validated correlated-k model for the longwave. *J. Geophys. Res.*, **102** (D14), 16663–16682.

Olson, D. A., N. W. Junker, and B. Korty, 1995: Evaluation of 33 years of quantitative precipitation forecasting at NMC. *Wea. Forecasting,* **10**, 498–511.

Rozulmalski, R., 2006: WRF Environmental Modeling System User's Guide. NOAA/NWS SOO Science and Training Resource Coordinator Forecast Decision Training Branch, 89 pp. [Available from COMET/UCAR, P.O. Box 3000, Boulder, CO, 80307-3000].

Rutledge, S. A., and P. V. Hobbs, 1984: The mesoscale and microscale structure and organization of clouds and precipitation in midlatitude cyclones. XII: A diagnostic modeling study of precipitation development in narrow cold-frontal rainbands. *J. Atmos. Sci.*, **41**, 2949-2972.

Schwarzkopf, M. D., and S. B. Fels, 1985: Improvements to the algorithm for computing CO2 transmissivities and cooling rates. *J. Geophys. Res*., **90**, 541-550.

Schwarzkopf, M. D., and S. B. Fels, 1991: The simplified exchange method revisited: An accurate, rapid method for computations of infrared cooling rates and fluxes. *J. Geophys. Res*., **96**, 9075-9096.

Shin, H. S. and S. Y. Hong, 2011: Intercomparison of planetary boundary-layer parameterizations in the WRF model for a single day from CASES-99. *Boundary-Layer Meteorol.*, **139**, 261–281.

Skamarock, W. C., J. B. Klemp, J. Dudhia, D. O. Gill, D. M. Barker, W. Wang, and J. G. Powers, 2005: A description of the Advanced Research WRF Version 2. NCAR Technical Note NCAR/TN-468+STR, 88 pp.

Tao, W. K., J.J. Shi, S. S. Chen, S. Lang, P. L. Lin, S. Y. Hong, C. Peters-Lidard, and A. Hou, 2011: The impact of microphysical schemes on hurricane intensity and track. *Asia-Pacific J. Atmos. Sci.*, **47**, 1-16.

Troen, I. and L. Mahrt, 1986: A simple model of the atmospheric boundary layer: Sensitivity to surface evaporation. *Bound.-Layer Meteor.*, **37**, 129–148.

List of Acronyms

AMU	Applied Meteorology Unit
ARW	Advanced Research WRF
CCAFS	Cape Canaveral Air Force Station
EMS	Environmental Modeling System
ER	Eastern Range
GFS	Global Forecast System
KSC	Kennedy Space Center
LIS	Land Information System
ME	Mean Error
MODE	Method for Object-Based Diagnostic Evaluation
MRF	Medium-Range Forecast
MYJ	Mellor-Yamada-Janjic
NAM	North American Mesoscale
NCAR	National Center for Atmospheric Research
NCEP	National Centers for Environmental Prediction
NMM	Non-hydrostatic Mesoscale Model
PBL	Planetary Boundary Layer
Ri	Richardson number
RMSE	Root Mean Square Error
RUC	Rapid Update Cycle
SOO	Science and Operations Officer
SPoRT	Short-term Prediction Research and Transition Center
SST	Sea Surface Temperature
STRC	Science and Training Resource Center
TKE	Turbulent Kinetic Energy
WDM6	WRF Double-Moment 6-Class
WFF	Wallops Flight Facility
WRF	Weather Research and Forecasting
WSM6	WRF Single-Moment 6-Class
WSR-88D	Weather Surveillance Radar-1988 Doppler
XMR	CCAFS rawinsonde 3-letter identifier
YSU	Yonsei University

NOTICE

Mention of a copyrighted, trademarked or proprietary product, service, or document does not constitute endorsement thereof by the author, ENSCO Inc., the AMU, the National Aeronautics and Space Administration, or the United States Government. Any such mention is solely for the purpose of fully informing the reader of the resources used to conduct the work reported herein.